SPATIAL RAINBOWS AND CATASTROPHES IN TRANSMISSION OF PROTONS THROUGH ELECTROSTATIC HEXAPOLE LENS

by

Igor N. TELEČKI [*]***, Sanja M. GRUJOVIĆ ZDOLŠEK, Petar D. BELIČEV, Srdjan M. PETROVIĆ, and Nebojša B. NEŠKOVIĆ***

Laboratory of Physics, Vinča Institute of Nuclear Sciences, University of Belgrade, Belgrade, Serbia

Scientific paper
http://doi.org/10.2298/NTRP1803231T

This work reports on the spatial rainbows occurring in transmission of 10 keV protons through hexapole lens. Positive potentials of the lens electrodes are set to be 0.9, 2, and 5 kV. The spatial rainbows and corresponding proton distributions are calculated by using an accurate analytical approximation of the numerically obtained lens potential. Further, for the positive potential of the lens electrode equal to 0.9 kV, it has been shown that application of catastrophe theory leads to a simple polynomial non-linear mapping, generating accurate spatial rainbows at the exit and in the drift space behind the lens.

Key words: hexapole, beam optics, catastrophe theory, rainbow line, aberration

INTRODUCTION

Electrostatic hexapole lens is an ion beam optics element consisting of six electrodes being on the alternating electrostatic potentials $\pm V_0$, that form a hexagon around the optical axis. The medium transverse position (TP) plane of the lens is shown in fig. 1. It is well known that the electrostatic potential of a hexapole lens around the optical axis is purely anharmonic, *i. e.*, its linear and parabolic parts are equal to zero [1, 2]. This implies that the second-order effects of a hexapole lens can be used to correct the ion beam aberrations without changing the first-order focusing conditions. Therefore, in ion beam optics, the main applications of hexapole lenses are the aberration corrections [3]. Reduction of the second-order image aberration for mass spectrometers, by using the electrostatic hexapole lens, was reported in [4, 5]. Further, the application of hexapole lens correctors for the three order image aberration (the spherical aberration), in the scanning and transmission electron microscopes, was investigated in [6, 7]. Trajectories of charged particles, in the electrostatic hexapole lens, have been calculated in details by Taya and Matsuda [2].

Recently, our group has been investigating the focusing and accelerating properties of the square lens with all electrodes being on the positive potential [8-11]. It was shown that the rainbow effect occurred for these lenses and strongly influenced their focusing and accelerating properties. We called the lens the square rainbow lens [8].

In this work, occurrence of the spatial rainbows, in transmission of 10 keV protons, through electrostatic hexapole lenses, with the alternating electrode potential $\pm V_0$, for V_0 = 0.9, 2, and 5 kV, are investigated. In addition, it is shown that catastrophe theory can be used to model the spatial rainbows for V_0 = 0.9 kV.

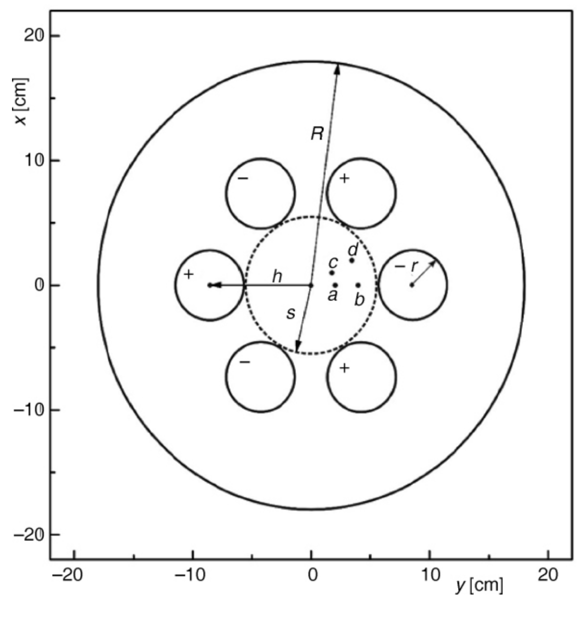

Figure 1. The medium transverse position plane of the hexapole lens

* Corresponding authors; e-mail: tigor@vin.bg.ac.rs

THEORY

Since a hexapole lens has straight axis, positive orientation of Cartesian coordinate system is chosen, being defined in fig 1. It can be shown that the hexapole lens potential can be approximated by a 2-D polynomial expression [2]. The imposed symmetry conditions on the 2-D hexapole potential, together with the fact that the Laplace's equation must hold, results in the following expression for the potential (up to the sixth order) [2]

$$\varphi(x, y) = \frac{V_0}{s_0^3}(y^3 - 3yx^2) \tag{1}$$

where, V_0 denotes the applied positive electrode potential and s_0 the radius of a circle inscribed within the six electrodes (see fig. 1). Also, it can be shown that the expression (1) is the best possible approximation for the realistic potential if one sets the radius of the electrodes to be: $r = s_0/2$ [2].

In this work, the potential given by expression (1) is considered. Further, in order to check its accuracy and applicability, the hexapole potential was calculated numerically. The numerical calculation was carried out applying the WIPL-D program [12], which is based on the method of moments with the Galerkin test procedure finite element method. The accuracy of calculation was determined by choosing the number of the linear algebraic equations, N, within the program. This number was chosen to be $N = 2{,}913$. It should be mentioned, that due to the symmetry of the lens, the computation was performed in the quadrant defined by $x = [0, 116 \text{ mm}]$, $y = [0, 116 \text{ mm}]$, and $z = [0, 400 \text{ mm}]$. Also, the computational mesh was defined by $\Delta x = \Delta y = 1$ mm and $\Delta z = 2$ mm.

Let us consider the mapping

$$(x_0, y_0) \to (x, y) \tag{2}$$

where x_0 and y_0 are the proton spatial components in the impact parameter (IP) plane, x and y are the proton spatial components during its motion through the lens and/or after it, at the transversal position (TP) plane. Proton spatial components in the TP plane are determined numerically by using the Runge-Kutta method of the fourth order for calculation of the proton trajectory [13].

The mapping (2) is presented with the following pair of functions: $x = x(x_0, y_0)$ and $y = y(x_0, y_0)$. In order to investigate the characteristic features of these functions, the following Jacobian is introduced: $J_\rho \overset{\text{def}}{=} \partial_{x_0}x\partial_{y_0}y - \partial_{x_0}x\partial_{y_0}y$. It is geometrically well known that the Jacobian can be interpreted via the relation, $J = \mathrm{d}x\mathrm{d}y/\mathrm{d}x_0\mathrm{d}y_0$, where $\mathrm{d}x_0\,\mathrm{d}y_0$ and $\mathrm{d}x\mathrm{d}y$ are elementary areas in the IP and TP planes, respectively.

Spatial rainbow lines in the IP plane are defined as solutions of the equation: $J = 0$. The spatial rainbow lines in the TP plane are determined by applying the mapping (2) to the spatial rainbow lines in the IP plane. Geometrical interpretation of the Jacobian implies that one can expect focusing properties of the beam around spatial rainbow lies in the TP plane, due to the fact that $\mathrm{d}x\mathrm{d}y \to 0$ as $J \to 0$, whereas $\mathrm{d}x_0\,\mathrm{d}y_0$ is constant. Further, if the Jacobian is equal to zero, then the mapping (2) is not one-to-one (bijective) and *vice versa*. Therefore, there is an abrupt (catastrophic) change along the rainbow line, which serves as the border between the so called bright and dark sides of the rainbow *i.e.* between the regions of high and low intensity of protons, respectively [8-11].

RESULTS AND DISCUSSION

In our calculations, we set for the radius of electrodes, $r = 2.82$ cm, the length of the lens, $L = 40$ cm, the radius of the circle inscribed within the electrodes, $s_0 = 2r = 5.64$ cm, and for the radius of the grounded cylinder of the lens, $R = 20$ cm (see fig. 1). The initial proton kinetic energy is taken to be $E = 10$ keV, whereas the initial number of protons is 400 000. The initial proton beam is parallel and the protons are assumed to be homogenously distributed within the circle of diameter equal to 5.5 cm, which is determined by the circular apertures in the entrance and exit plates, with the same diameter equal to 5.5 cm. The origin of the used coordinate system is taken to be in the middle of the lens. The horizontal and vertical co-ordinates, y and x, respectively, are chosen so that the proton beam is directed toward positive direction of z-axis, which coincides with the lens axis. The entrance and exit transversal planes correspond to the longitudinal coordinate $z = -21.5$ cm and $z = 21.5$ cm, respectively. It should be noted that the IP plane coincides with the entrance plane in the case of potential (1), whereas for the numerically calculated potential it corresponds to $z = -40$ cm, when the potential can be approximated by zero.

Figure 1 shows the characteristic points in the medial plane of the lens designated by a, b, c, and d. Their co-ordinates are: (2 cm, 0), (4 cm, 0), (1.73 cm, 1 cm), and (3.46 cm, 2 cm), respectively. They will be used for the comparison between the numerically calculated electrostatic field and the one obtained from the analytical potential (1).

Dependencies of the numerically calculated components of electrostatic fields, E_x, E_y, and E_z and the corresponding analytical components, E_x^a, E_y^a, and E_z^a, on the co-ordinate z, for the points a, b, c, and d, are shown in figs. 2(a-d), respectively. The potential of an electrode is taken arbitrary to be, $V_0 = 1$ V. It is clear, from fig. 2, that the transversal components of the electrostatic field E_x^a and E_y^a excellently approximate the components E_x and E_y, inside the lens. Further, inside the lens, E_z is close to zero, whereas the E_z^a component is exactly equal to zero, which follows from the fact that the potential (1) does not depend on z. Thus, small differences between the analytical and

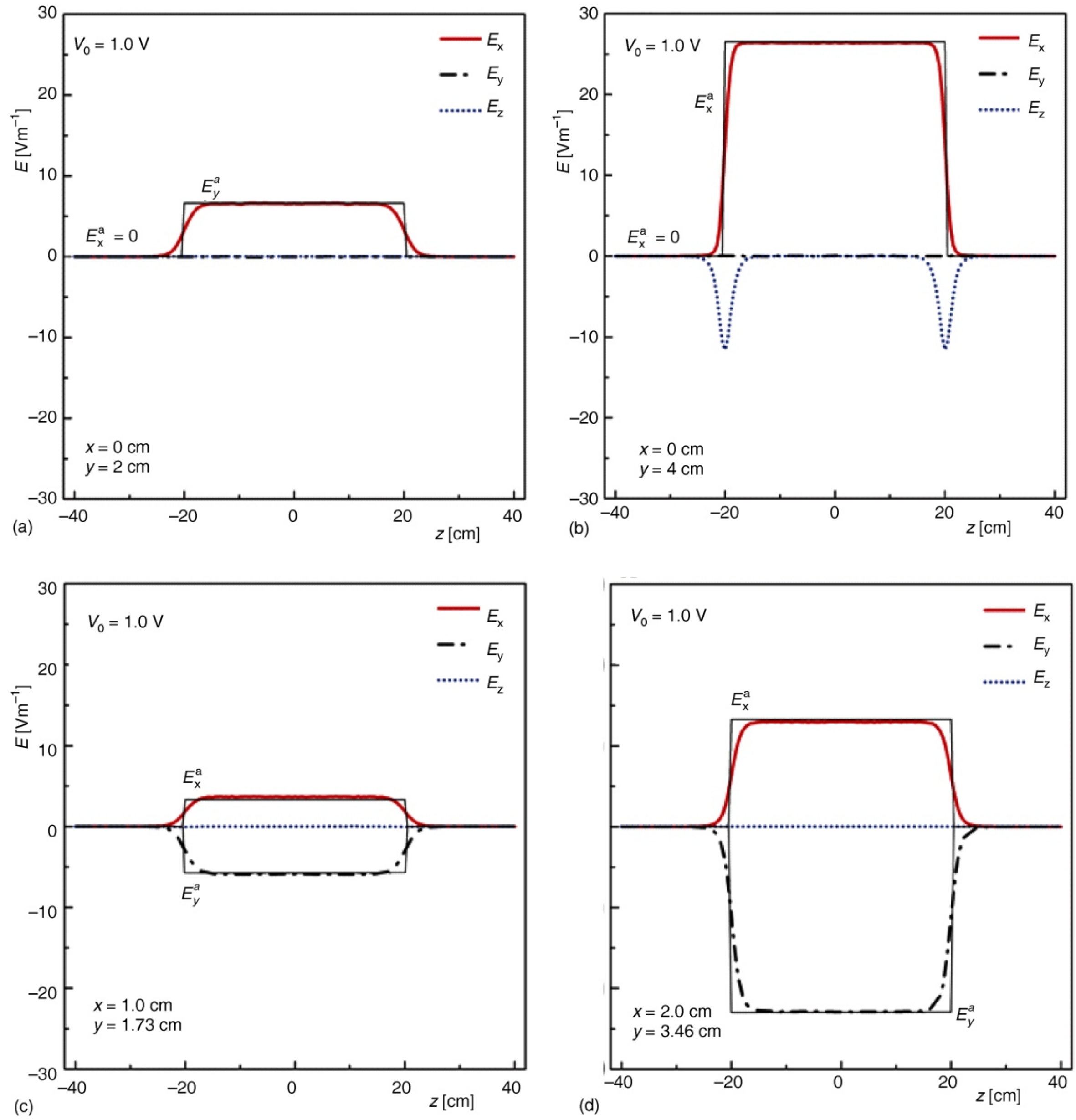

Figure 2. Dependences of the numerical, E_x, E_y, and E_z, and analytical, E_x^a, E_y^a, and E_z^a, components of the electric fields, on the variable z, for transverse positions corresponding to (a) point a, (b) point b, (c) point c, and, (d) point d, in fig. 1

numerical electrostatic fields occur in the entrances and exit regions of the lens edges since the numerical electrostatic field includes the fringe fields effect. However, on ref. [14] it was shown that the contribution of the fringe field effect in a hexapole lens was in the order of $(s_0/L)^2$. In our case, $(s_0/L)^2 = 0.005$, which is very small (an order of a half percent). Moreover, fig. 3 shows, for the positive electrode potential, $V_0 = 0.9$ kV, that the rainbow lines obtained from the numerical calculation, designated by red color, and the analytical one, designated by green color, are very close to each other. (Alternative gray and dark colors are used in printed version of the journal). Therefore, the fringe field effects could be neglected and the 2-D potential (1) has been applied further in the text. As a consequence, as it has been already mentioned, the IP plane coincides with the entrance aperture plane of the lens, and the drift space approximation holds for z 21.5 cm, *i. e.*, the proton trajectories are treated as the straight lines after they exit the lens.

Figures 4(a, b) show the closed rainbow lines in the IP plane and the corresponding rainbow lines and spatial distributions of transmitted protons in the exit TP of the lens, for the electrode potential $V_0 = 0.9$ kV, respectively. The red and green (gray and dark) points designate the focused and defocused protons, respectively. The proton is treated as focused if it satisfies the condition $xv_x + yv_y$ 0, where v_x and v_y are the transverse co-ordinates of the ion velocity [5]. Otherwise, it is defocused. In the calculation, it is assumed that protons, being in the areas inside the electrodes, or not passing through the exit aperture, are not taken into

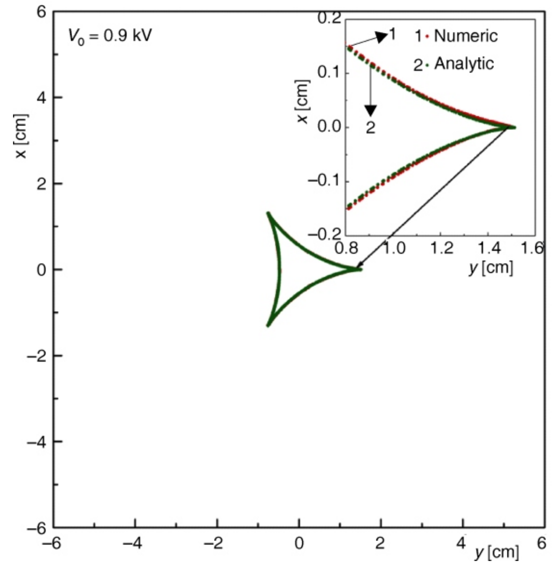

Figure 3. The red and green (gray and dark) points designate analytical and numerical rainbow lines, respectively, at the exit of hexapole lens for the positive potential of the lens, $V_0 = 0.9$ kV

account. The same assumption holds for the rainbow lines. Figure 4(b) shows the cusped triangular rainbow line with the cusps being directed toward negative electrodes of the lens. It is clear that the shape of the distribution is determined with the rainbow line, *i. e.*, it acts as a "skeleton" of the distribution. Also, it is the border between the "bright side" and the dark side of the rainbow, corresponding to high and low proton yield, respectively. Further, focused protons are confined within this rainbow line, whereas the defocused protons are concentrated in the areas around the cusps of the rainbow line.

For the electrode potential $V_0 = 2.0$ kV, figs. 4(c) and 4(d) show that the second rainbow lines, in the IP and exit TP planes, appear whereas the first rainbow lines are becoming smaller in both of the planes – in comparison with the cases presented in figs. 4(a) and 4(b). Also, the focused protons are confined within the first cusped triangular rainbow line and in three areas close to the second rainbow line directed toward the positive electrodes of the lens.

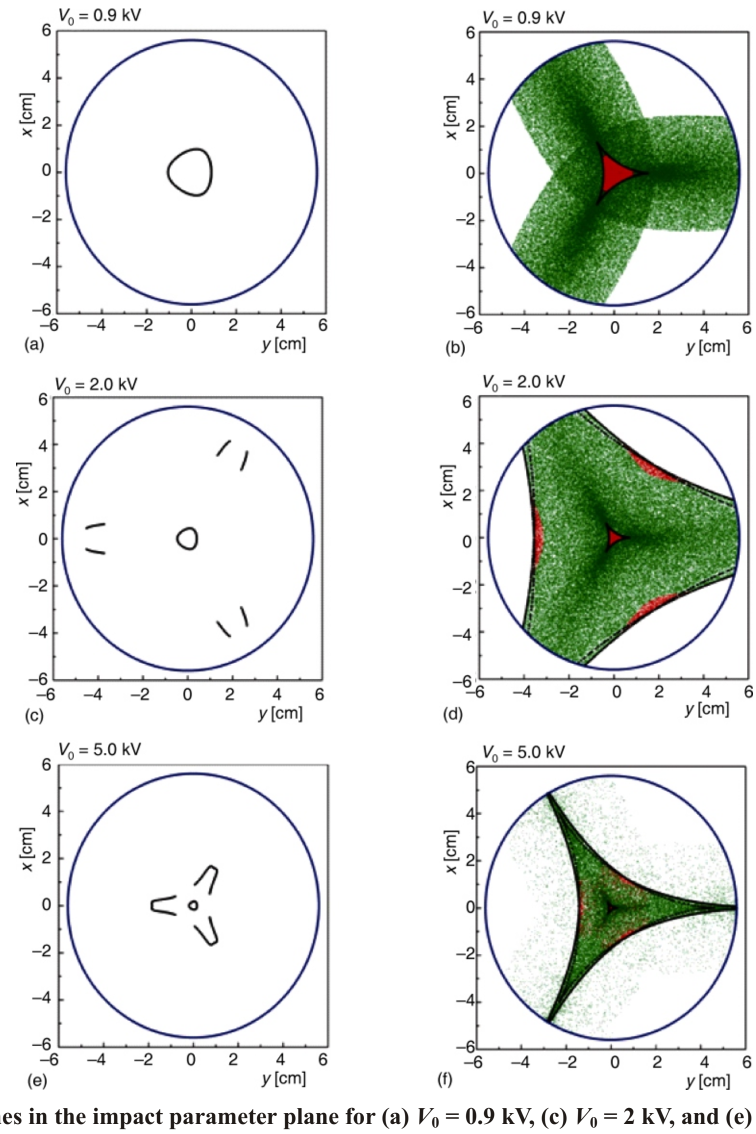

Figure 4. Rainbow lines in the impact parameter plane for (a) $V_0 = 0.9$ kV, (c) $V_0 = 2$ kV, and (e) $V_0 = 5$ kV, and corresponding distribution of protons in the exit transverse plane for (b) $V_0 = 0.9$ kV, (d) $V_0 = 2$ kV, and (f) $V_0 = 5$ kV where the red and green (gray and dark) points designate focused and defocused protons, respectively

Figure 4(e) and 4(f) show the rainbow lines in the IP plane and the corresponding rainbow lines and the spatial distribution of transmitted protons in the exit TP of the lens, for the electrode potential V_0 = 5 kV. Figure 4(d) confirms the given conclusion, that the second rainbow lines define the shape or "skeleton" of the beam at the exit of the lens and that the focused protons are confined within the first cusped triangular rainbow line and in three areas close to the second rainbow lines, directed toward the positive electrodes. Further, it is clear that the second rainbow lines consist of parts of one almost closed cusped rainbow line, with two pairs of cusps being directed toward the negative electrodes of the lens.

Evolution of the spatial rainbow lines in the drift space for the electrode potential V_0 = 2 kV, for the variable z = 21.5, 40, 70, and 120 cm, is presented in fig. 5(a). Interestingly, this evolution shows that the first rainbow line decreases, as the variable z increases, but, on the other hand, the outer parts of the second rainbow line are joining together to form one single secondary rainbow line, which increases as the variable z increases. Figure 5(b) shows enlarged the evolution of the first rainbow line for the given values of variable z. It is clear from fig. 5(a) and (b) that, for the large distances from the lens, the first rainbow line tends to a point, keeping its shape, and the spatial distribution of the proton beam has been determined by the second rainbow line only.

In general, catastrophe theory is a mathematical theory of structurally stable family of functions, that can be used in physics and other branches of science as a tool for obtaining the simple polynomial models of the processes under the investigations [15]. In its application, it is implicitly assumed that the processes are structurally stable, *i. e.*, that they are not sensitive to small perturbations. In further parts of this work, the results of application of catastrophe theory to the spatial rainbows and the corresponding proton distributions for V_0 = 0.9 kV, will be presented.

Let us introduced the generating function

$$F(x_0, y_0; x, y, z) \quad \frac{1}{2}(x_0^2 \quad y_0^2) \quad \frac{1}{3}a(z)(y_0^3 \quad 3y_0x_0^2) \quad \frac{1}{4}b(z)(x_0^2 \quad y_0^2)^2 \quad x_0x \quad y_0x \tag{3}$$

The first term corresponds to the linear one in the mapping defined by eqs. (4) and (5), the second and third terms correspond to elliptic umbilic and rotational cusp catastrophes [15, 16], or the X_9 catastrophe when its modulus is equal to 2 [17, 18]. It should be noted that the second term of the generating function is related to the astigmatism of the second order, whereas the third term is related to the spherical aberration of the third order [16].

The generating function defines the following polynomial non-linear mapping, $x_0, y_0 \quad x, y$, via the relations

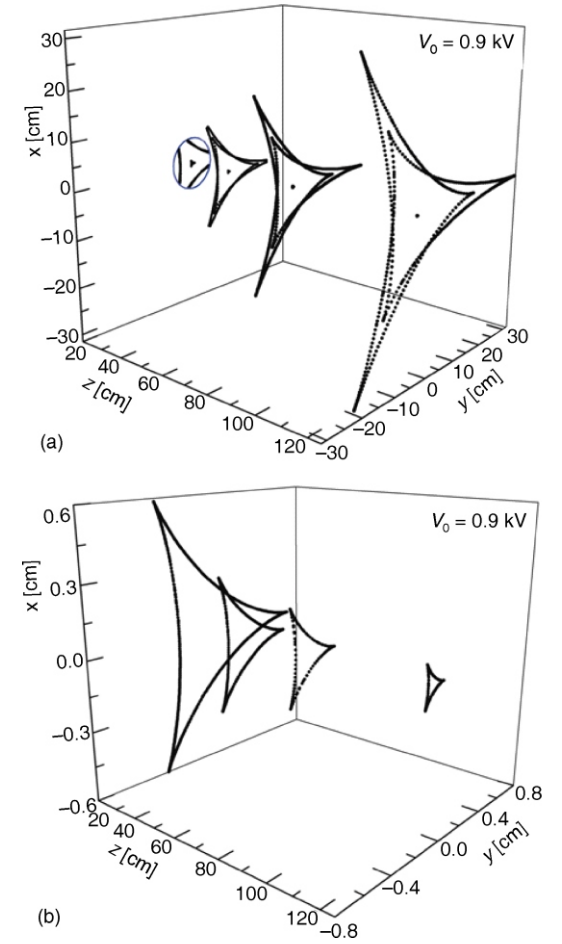

Figure 5. (a) Rainbow lines in the transverse plane for z = 21.5, 40, 70, and 120 cm, and (b) enlarged first rainbow lines presented in (a)

$$\partial_{y_0}F(x_0, y_0; x, y, z) \quad 0 \quad y \quad y_0 \quad a(z)(y_0^2 \quad x_0^2) \quad b(z)y_0(x_0^2 \quad y_0^2) \tag{4}$$

$$\partial_{x_0}F(x_0, y_0; x, y, z) \quad 0 \quad x \quad x_0 \quad 2a(z)x_0y_0 \quad b(z)x_0(x_0^2 \quad y_0^2) \tag{5}$$

According to catastrophe theory, the conditions (4) and (5) define the equilibrium set of the family of functions F [15]. It can be shown that the Jacobian of the 2-D mapping, defined with (4) and (5), is given by

$$J_\rho(x_0, y_0; x, y, z) \quad \partial_{x_0}^2 F \partial_{y_0}^2 F \quad (\partial_{x_0}\partial_{y_0}F)^2 \quad 1 \quad 4y_0^2[b(z) \quad a^2(z)] \quad 4x_0^2[b(z) \quad a^2(z)] \quad 4a(z)b(z)y_0^3 \quad 12a(z)b(z)y_0x_0^2 \quad 3b^2(z)y_0^4 \quad 3b^2(z)x_0^4 \quad 6b^2(z)x_0^2y_0^2 \tag{6}$$

which represents, on the other hand, the Hessian of generating function, $H(F)$ [15]. According to catastrophe theory, equation, $H(F)$ = 0, which is equivalent to the condition defining the spatial rainbow lines in the IP plane, corresponds to the catastrophic set of the family of functions F. Bifurcation set of the family F is defined as the mapping of the catastrophic set via the equations (4) and (5) [15], and, therefore, corresponds to the rainbow lines in TP plane. Thus, we have shown a direct connection between the rainbow lines in the IP and TP planes and the catastrophic and bifurcation sets of the generating function (3), respectively.

Figure 6(a and b) show the model rainbow lines obtained by applying the mapping black line (4) and (5) and the numerically calculated red (gray) line ones in the IP and TP planes, respectively, for $z = 43$ cm. The parameters a and b are determined in the fitting procedure, which obtains the best matching between the corresponding numerical and model rainbow lines, in both IP and TP planes. This is achieved by minimizing the sum of squared distances between corresponding points 1 and 1_m, 2 and 2_m, 1′ and $1'_m$, and, 2′ and $2'_m$, presented in figs. 6(a and b). The same procedure is applied for the values of variable z = 50, 60, 70, 80, 90, 100, 120, and 140 cm, in the drift space. This is illustrated in figs. 6(c) and (d) for $z = 90$ cm. One can conclude that the matching between the numerical and model rainbow lines, in both IP and TP planes, is excellent.

The obtained values of parameters a and b are presented in figs. 7(a and b), respectively. The analysis shows that dependences of parameters a and b on variable z can be excellently fitted with the following analytical functions, $a(z) = a_1 - a_2 \exp(-z/a_z)$ and $b(z) = b_1 - b_2 \exp(-z/b_z)$, respectively. Calculated parameters of the fitting functions are: $a_1 = 0.26$ cm^{-1}, $a_2 = 0.54$ cm^{-1} and $a_z = 29.10$ cm, and $b_1 = 0.09$ cm^{-2}, $b_2 = 0.25$ cm^{-2} and $b_z = 37.18$ cm.

CONCLUSIONS

In this work, it is shown that the spatial rainbows occur in transmission of 10 keV protons through the

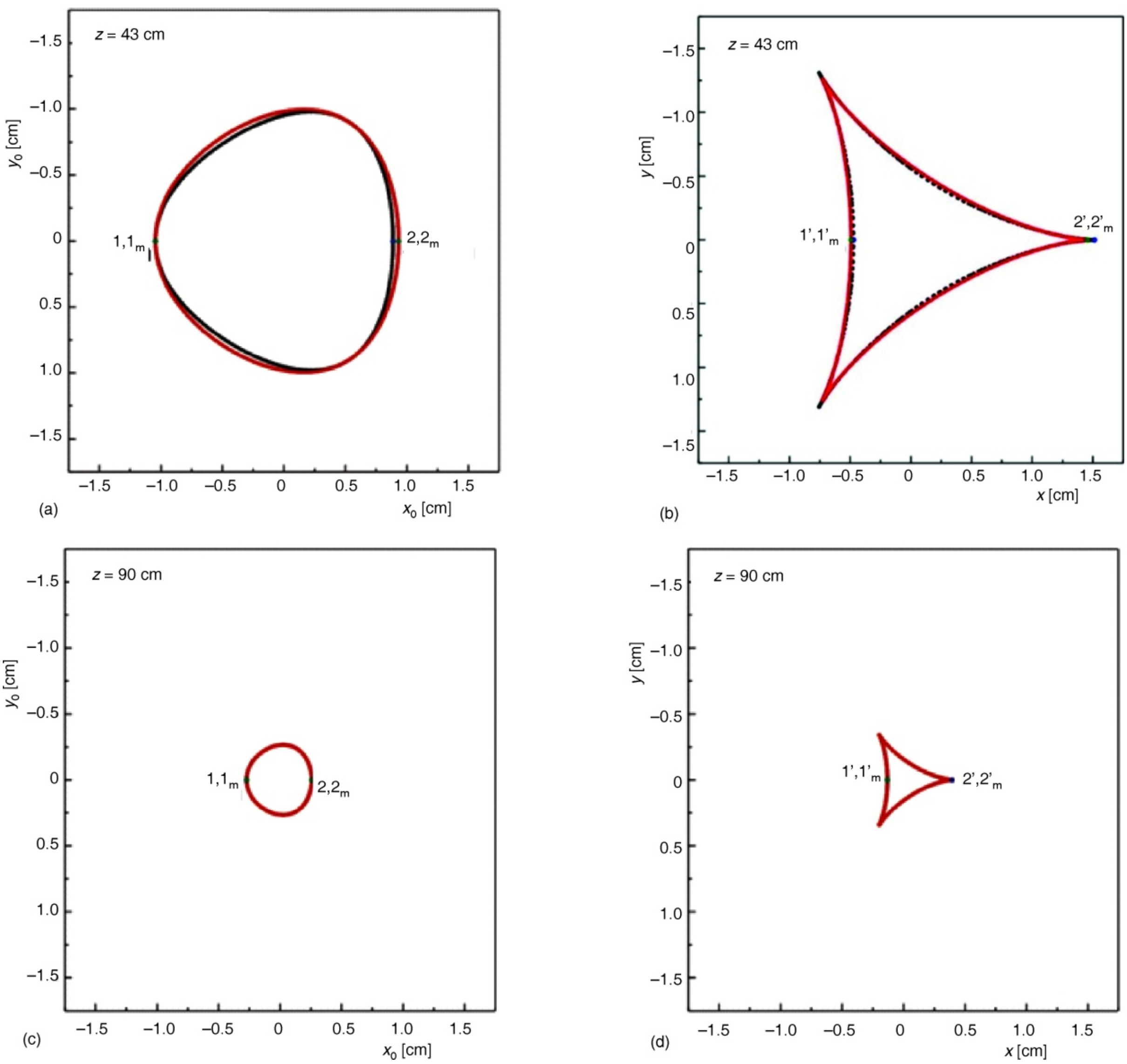

Figure 6. Numerical and polynomial model of rainbow lines for show, respectively, in red and black (gray and black) colors for (a) $z = 43$ cm and (c) 90 cm, in the impact parameter plane, and in the transverse position planes, for (b) $z = 43$ cm and (d) 90 cm

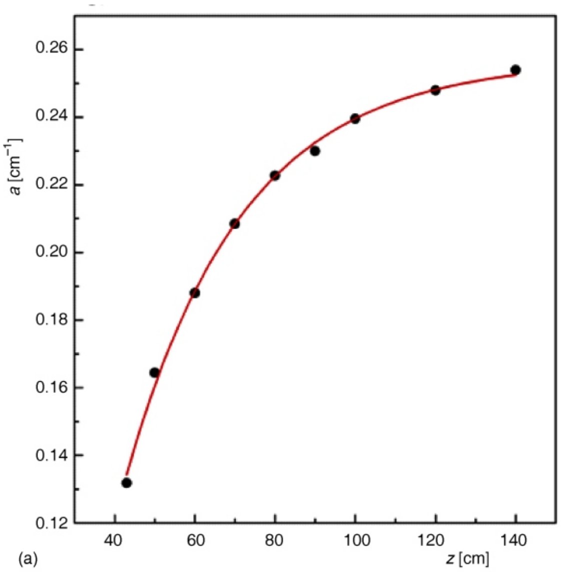

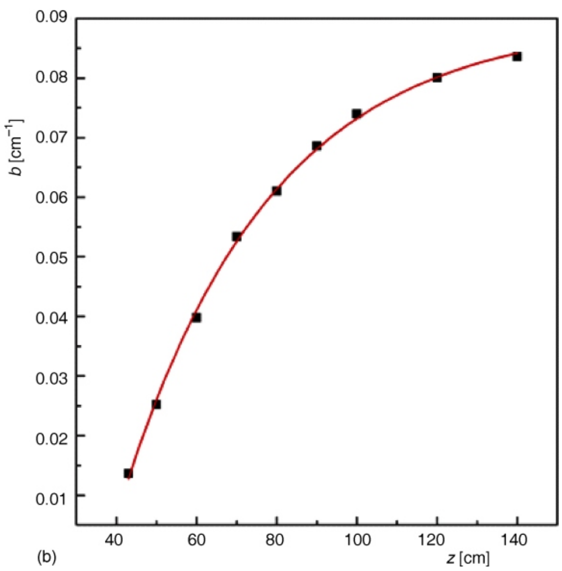

Figure 7. Dependencies of the fitting parameters (a) *a*, and (b) *b*, on the variable *z*

hexapole lens having positive potentials $V_0 = 0.9$, 2.0, and 5.0 kV. They represent "skeletons" of the spatial distributions and borders between the "bright sides" and the "dark sides" of the rainbows, corresponding to high and low proton yields, respectively. Further, focused protons are confined within first rainbow line, whereas the defocused protons are concentrated in the areas around the cusps of the first rainbow line.

Applying catastrophe theory, for the positive potential of the electrode, $V_0 = 0.9$ kV, the analysis shows that one can obtain simple non-linear mapping from the IP to TP plane, that excellently model the numerically calculated spatial rainbow lines. Additionally, dependence of the parameters of the mapping, *a* and *b*, on the variable *z*, can be excellently fitted with the exponential functions $a(z) = a_1 - a_2 \exp(-z/a_z)$ and $b(z) = b_1 - b_2 \exp(-z/b_z)$, where $a_1 = 0.26$ cm^{-1}, $a_2 = 0.54$ cm^{-1} and $a_z = 29.10$ cm, and $b_1 = 0.09$ cm^{-2}, $b_2 = 0.25$ cm^{-2} and $b_z = 37.18$ cm.

ACKNOWLEDGMENT

We acknowledge the support to this work provided by the Ministry of Education, Science and Technological Development of Serbia through the project Physics and Chemistry with Ion Beams, No. III 45006.

AUTHORS' CONTRIBUTIONS

The idea for this research was initiated by N. B Nešković. Computations were carried out by I. N Telečki, P. D. Beličev, and S. G. Grujović Zdolšek. The manuscript was written by I. N. Telečki, S. M. Petrović, and P. D. Beličev.

REFERENCES

[1] Boerboom, A. J. H., Ion Optics of the Electric Hexapole, *Int. J. Mass. Spectr. Ion Phys., 8* (1972), 5, pp. 475-492
[2] Taya, S., Matsuda, H., A Third Order Transfer Matrix of an Electrostatic Hexapole Lens. Int., *J. Mass Spectr. Ion Phys., 9* (1972), 3, pp. 235-245
[3] Carey, D. C., The Optics of Charged Particle Beams (Harwood Academic Publishers, Chur. London. Paris, New York, 1987, p. 298
[4] Tang, T. T., Correction of Aberrations in a Magnetic Spectrometer by Electric Multipole Lenses, *Ultramicroscopy, 7* (1982), 4, pp. 305-310
[5] Hawkes, P. W., The Correction of Electron Lens Aberrations, *Ultramicroscopy, 156* (2015), March, pp. 1-64
[6] Taya, S., *et al.*, Second-Order Image Aberration Correction of Double-Focusing Mass Spectrometers by Electrostatic Hexapole Lens, *Nucl. Instrum. Meth., A 152* (1978), June, pp. 407-414
[7] Rose, H., Correction of Aperture Aberrations in Magnetic Systems with Threefold Symmetry, *Nucl. Instrum. Meth., 187* (1981),1, pp. 187-199
[8] Nešković, N., *et al.*, A Square Electrostatic Rainbow Lens: Catastrophic Ion Beam Focusing, *Nucl. Instrum. Meth. A, 635* (2011),1, pp. 1-7
[9] Telečki, I., *et al.*, Focusing Properties of a Square Electrostatic Rainbow Lens, *Nucl. Instr. Meth., A 694* (2012), Dec., pp. 224-233
[10] Nešković, N., *et al.*, Rainbow Lenses, *Advances in Imaging and Electron Physics, 182* (2014), Apr., pp. 123-186
[11] Telečki, I., *et al.*, Focusing Properties of a Square Electrostatic Rainbow Lens Doublet, *Nucl Technol Radiat, 30* (2015), 4, pp 239-248
[12] ***, WIPL-D, 3-D Electromagnetic Solver Professional Edition, Belgrade, 2009
[13] Press, W. H., *et al.*, Numerical Recipes in FORTRAN, Cambridge University Press, Cambridge, UK, 1993
[14] Taya, S., Matsuda, H., Third Order Transfer Matrices for the Fringing Fields of an Electrostatic Hexapole Lens, *Mass Spectroscopy, 19* (1971), Dec., pp. 266-273
[15] Gilmore, R., Catastrophe Theory for Scientist and Engineers, John Wiley & Sons, New York, 1981

[16] Rose, H., Geometrical Charged-Particle Optics, Springer-Verlag, Berlin, Heidelberg, 2013
[17] Nešković, N., *et al*., The X9 Catastrophe as the Organizing Center of Crystal Rainbows, *Physics Letters A, 179* (1993), 6, pp. 343-347
[18] Nye, J. F., Natural Focusing and Fine Structure of Light, Institute of Physics, Bristol, UK, 1999

Received on February 19, 2018
Accepted on April 26, 2018

Игор Н. ТЕЛЕЧКИ, Сања М. ГРУЈОВИЋ ЗДОЛШЕК, Петар Д. БЕЛИЧЕВ, Срђан М. ПЕТРОВИЋ, Небојша Б. НЕШКОВИЋ

ПРОСТОРНЕ ДУГЕ И КАТАСТРОФЕ У ТРАНСМИСИЈИ ПРОТОНА КРОЗ ЕЛЕКТРОСТАТИЧКО ХЕКСАПОЛНО СОЧИВО

У раду су приказане просторне дуге које се јављају при трансмисији снопа протона енергије 10 keV кроз хексаполно сочиво. Позитивни потенцијали електрода су били 0,9, 2, и 5 kV. Просторне дуге и одговарајуће расподеле протона рачунате су коришћењем прецизне аналитичке апроксимације нумерички добијеног потенцијала сочива. Касније, за позитиван потенцијал електроде хексапола 0.9 kV, показано је да примена теорије катастрофе доводи до једноставног полиномног, нелинеарног пресликавања, које генерише тачне просторне дуге на излазу и у слободном простору иза сочива.

Кључне речи: хексапол, јонска оптика, теорија катастрофе, линија дуге, аберација